J Mater Sci (2006) 41:4532–4536
DOI 10.1007/s10853-006-0091-y

Fabrication of nanostructures with different iron concentration by electron beam induced deposition with a mixture gas of iron carbonyl and ferrocene, and their magnetic properties

M. Takeguchi · M. Shimojo · K. Mitsuishi · M. Tanaka · R. Che · K. Furuya

Received: 28 November 2005 / Accepted: 8 February 2006 / Published online: 28 June 2006

Abstract Electron beam induced deposition (EBID) with a mixture gas of iron carbonyl and ferrocene was carried out to fabricate nanostructures with different iron concentrations in a chamber of a scanning electron microscope. The iron concentration was controlled by changing the ratio of partial pressure of iron carbonyl and ferrocene. Electron holography observation revealed that the remanent magnetic flux density B_r values of the nanostructures were also changed depending on the iron concentration.

Introduction

Fabrication of nanometer-sized ferromagnetic structures with desired shapes has attracted much attention because of the interesting properties of such nanometer-sized magnetic materials and potential of application to not only ultrahigh density magnetic recording but also new nanometer-sized magnetic devices such as read heads and memory cells [1, 2]. Electron beam induced deposition (EBID) has become one of the most promising methods in point of view of its high resolution, abundant types of deposit elements, and capability of three-dimensional fabrications [3–10]. Recently, EBID with precursors containing magnetic elements such as iron and cobalt has been employed to fabricate ferromagnetic nanostructures [7, 11, 12].

In EBID, metal-organic gases are decomposed by electron beams, resulting in the deposition of metals at the desired positions. The deposits formed at room temperature are in the amorphous phase or a mixture of nanocrystals and amorphous phase, and they contain a considerable amount of carbon in addition to metal element [13–15]. This unfavorable carbon comes from ligands of the dissociated organic precursors, and how to control the carbon concentration has been a significant issue. For instance, although a heating treatment results in transformation from the as-deposited phase to crystalline one, a great deal of carbon causes the formation of carbide but not pure metal [14]. Only if the carbon concentration is sufficiently low, pure metal nanostructures can be obtained by the heating treatment [7, 15]. Furthermore, the compositional ratio of metal to carbon in EBID nanostructures significantly influences electronic and magnetic properties. In particular, the electronic properties depend on the metal concentration, and it is known that high resistivity and current–voltage non-linear characteristics appear in EBID nanostructures [16–20]. As for the magnetic properties, it has been reported that the remanent magnetic flux density B_r of iron contained nanostructures formed from iron carbonyl, $Fe(CO)_5$, were evaluated by electron holography [7]. However, no study about the relationship between the iron concentration and magnetic properties has been done so far.

In the present work, dual gas-introduction pipelines were installed into a scanning electron microscope (SEM) dedicated to EBID, and nanostructures with different compositional ratios of iron to carbon were formed using a mixture gas of iron carbonyl, $Fe(CO)_5$, and ferrocene,

M. Takeguchi (✉) · M. Shimojo · K. Mitsuishi · M. Tanaka · R. Che · K. Furuya
High Voltage Electron Microscopy Station, National Institute for Materials Science, 3-13 Sakura, Tsukuba 305-0003, Japan
e-mail: takeguchi.masaki@nims.go.jp

M. Shimojo
Advanced Science Research Laboratory, Saitama Institute of Technology, 1690 Fusaiji, Okabe-machi, Saitama 369-0293, Japan

$Fe(C_5H_5)_2$. Stoichometrically, the ratio of iron to carbon of $Fe(CO)_5$ is twice as many as that of $Fe(C_5H_5)_2$. Using this dual gas EBID system, the iron-to-carbon compositional ratio in the EBID nanostructures was successfully controlled by changing the partial pressure of these gases. The iron and carbon concentration in the nanostructures was measured by energy dispersive X-ray spectrometer (EDS) and their magnetic properties were evaluated by electron holography. The dependency of the magnetic properties of the EBID nanostructures on the iron-to-carbon compositional ratio was described.

Experiment

A 30-kV ultrahigh vacuum SEM equipped with a field emission gun (JEOL JSM-7800FV), of which base pressure was less than 1×10^{-6} Pa, was employed to carry out EBID fabrication. A schematic illustration of the deposition experiment was shown in Fig. 1. A gas introduction system combined with dual gas source reservoirs and pipelines through leak valves was installed into the SEM so that the partial pressure of two kinds of gases could be independently controlled and their mixture could be introduced into a specimen chamber of the SEM via a nozzle with a inner diameter about 0.2 mm. The nozzle tip was about 1 mm from the electron beam position. A molybdenum substrate was partly thinned by a focused ion beam thinning system (JEOL JEM-9310FIB), and straight nanorods about 50 nm wide and 650–1100 nm long were formed on an edge of the thinned area at room temperature with various ratios of the partial pressure of iron carbonyl to ferrocene gases.

The electron beam current was about 0.8 nA with the beam diameter of 4 nm. To form free-standing nanorods, the electron beam position was moved from the substrate into an open space. The width and thickness of the nanorods depend on the deposition rate, which is determined by gas pressure, beam intensity, beam scan speed, dissociation energy of gas source, etc. [21]. It should be remarked that the deposition rate of the mixture gas changes depending on the mixture ratio because the dissociation energy for Fe-$(CO)_5$ bond (~6.0 eV [22]) is smaller than that of Fe–$(C_5H_5)_2$ bond (~6.8 eV [23]). Therefore, in the present work, for the various mixture ratios of iron carbonyl and ferrocene, the scan speed was controlled to make the width of the nanorods as uniform as possible.

Transmission electron microscopy (TEM) observation and off-axis electron holography were performed in a 300 kV field emission gun transmission electron microscope, JEOL JEM-3000F, equipped with an electron biprism. The objective lens was turned off during electron holography experiment and a mini objective lens located below the objective lens was used to form off-axis holograms on a Gatan ultrascan CCD camera integrated in a Gatan imaging filter.

Results and discussion

Figure 2a shows a SEM image of nanorods (numbered from 1 to 10) on an edge of a molybdenum thinned area formed by EBID with various partial pressures of iron carbonyl and ferrocene gases. First, the partial pressure of ferrocene gas was maintained at 1×10^{-5} Pa. Carbonyl gas was then introduced so that the total pressure was increased from 3×10^{-5} Pa to 12×10^{-5} Pa by 1×10^{-5} Pa for each

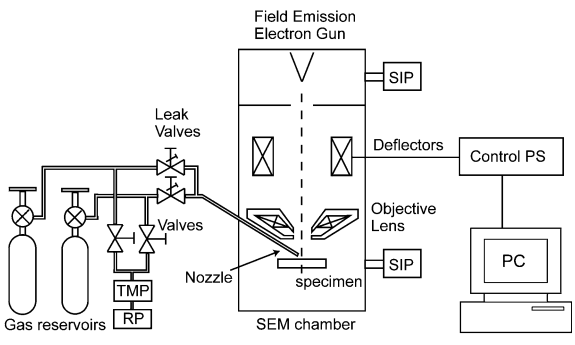

Fig. 1 Schematic drawing of a 30 kV FEG-SEM equipped with dual-gas introduction system for fabrication of the nanorods by EBID with a mixture gas of iron carbonyl and ferrocene

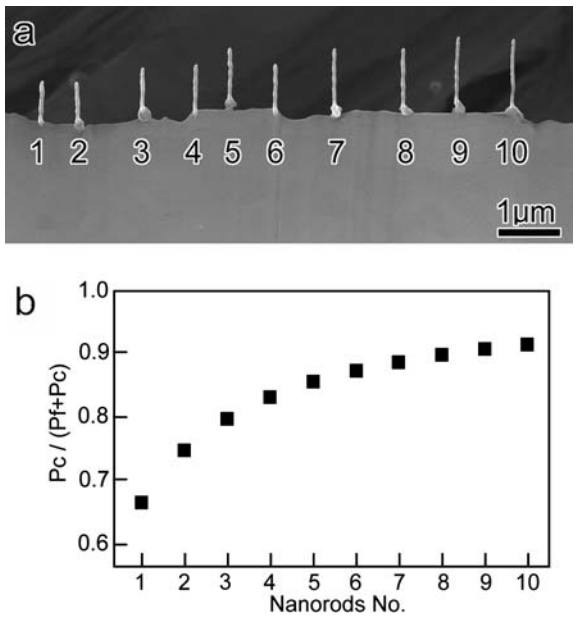

Fig. 2 SEM image of the EBID fabricated nanorods formed on an edge of a molybdenum thinned area. (**b**) The ratio of the partial pressure of carbonyl (P_c) to the sum of P_c and the partial pressure of ferrocene (P_f) for each nanorod

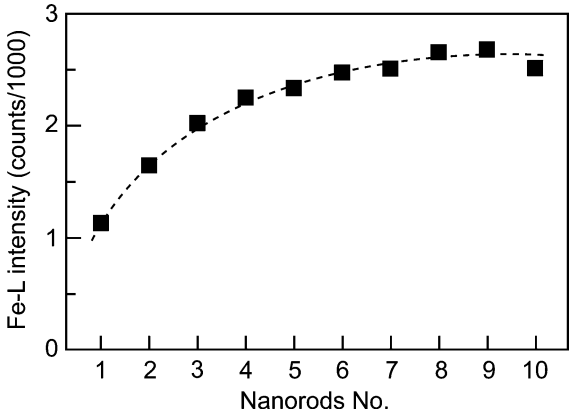

Fig. 3 The result of EDS analysis, showing Fe-L intensity for each nanorod

EBID fabrication of nanorod (in total 10 nanorods were formed). Figure 2b shows the ratio of the partial pressure of carbonyl (P_c) to the sum of P_c and the partial pressure of ferrocene (P_f) for each nanorod.

EDS analysis was performed to evaluate the iron concentration in the nanorods. Spectra acquired from several areas of each nanorod using a focused electron beam indicated that iron distributed homogenously in the nanorod body, which is consistent with the previous results [14]. Iron-L peak intensity for each nanorod is shown in Fig. 3, indicating that the iron concentration was successfully increased depending on the change of $P_c/(P_c+P_f)$ and the iron concentration was almost saturated for the No. 8–10 nanorods. The carbon-K peak was hardly detected because of the insensitivity and poor resolution of the current EDS detector. Previously reported EELS analysis showed that iron, carbon and oxygen contained in the nanorod formed by EBID with only iron carbonyl on the same beam condition as the present experiment was about 70, 10 and 20 at.%, respectively [15]. Roughly assuming that the iron concentration of the No. 8–10 nanorods is 70 at.% and the thickness of all the nanorods is the same, the iron concentration of the No. 1 nanorod was approximated to be 30%.

The remanent magnetic flux density B_r for each nanorod was evaluated by off-axis electron holography. Phase image was obtained by a digital reconstruction process as described in the literature [24]. Figure 4a and b show an electron hologram of the No. 3–6 nanorods and the corresponding reconstructed phase image, respectively. The phase image is displayed as an interference micrograph, in which dark fringes are equivalent to equi-potential contour lines. The spacing of the dark fringes corresponds to a phase shift of $\pi/2$ rad, because the phase image was reconstructed with an amplification factor of 4. A line profile of the phase across the line AA' in the No. 6 nanorod is shown in Fig. 4c. Since the hologram carrier fringes in the nanorod were overlapped with the nanorod TEM image, contrast of the fringes at the

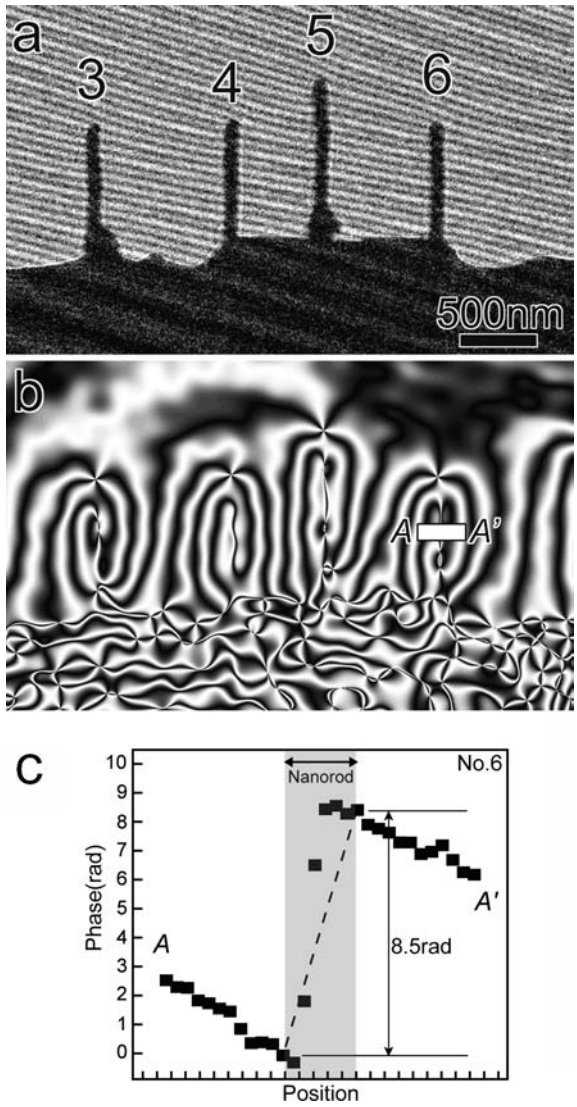

Fig. 4 (**a**) Electron hologram of the No. 3–6 nanorods. (**b**) Phase image (interference micrograph) reconstructed from (**a**) with an amplification factor of 4. (**c**) Line profile of the phase distribution across the line AA' in the No. 6 nanorod

nanorod position was too low to extract the phase information. Although the phase in the nanorod was unclear, it was possible to measure the phase jump across the nanorod, which was caused by internal magnetic flux [7], by measuring the phase at the positions adjacent to both side surfaces of the nanorod. For example, the phase jump for the No. 6 nanorod was about 8.5 rad as shown in Fig. 4c. The phase jump across the nanorod $\Delta\phi$ caused by the internal magnetic flux density B is described as

$$\Delta\varphi = 2\pi\frac{e}{h}BS \quad (1)$$

where S is a cross section area of the nanorod. However, the stray fields above and under the nanorod oriented in opposite

direction to the internal magnetic field should be taken into account to estimate the accurate magnetic flux in the nanorod [25], because the observed phase jump is actually the sum of the phase shift due to the internal magnetic field and the vertical integration of the magnetic stray fields at the nanorod position. The phase shift due to the stray fields at the nanorod position was extrapolated approximately from the phase distribution near the nanorod, and found to be around 1.6 rad for the No. 6 nanorod. This value is similar to the multiply factor of $\pi/2$ for the accurate determination of the magnetic flux in magnetized sphere [25]. Thus, for the No. 6 nanorod, the phase shift due to the internal magnetic flux BS was estimated to be about 10.1 rad, and the corresponding internal magnetic flux BS was about 6.6×10^{-15} Wb. In the same way as that one, the internal magnetic flux for other nanorods could be obtained.

In order to evaluate the magnetic flux density B (namely B_r, without applied outer magnetic field), the cross section area for the nanorods must be known. The shape of the cross section of the nanorod was supposed to be elliptic and the width of the nanorod was measured from TEM (or SEM) images. The thickness was estimated from 45° tilted SEM images, and the resultant values were in the range from 230 to 270 nm with a considerable margin of error. For more accurate evaluation of the thickness, intensity of Z-contrast image provided by high-angle annular dark-field scanning transmission electron microscopy (HAADF-STEM) were utilized as follows; The Z-contrast image intensity is proportional to the product of thickness and Z^{α} (Z: atomic number; α: ~1.7) [26]. The Z-contrast image intensity I is given as

$$I = aZ^{\alpha}t \tag{2}$$

where a is a constant and t is the thickness. In the present case, since the nanorods contain iron ($Z = 26$), carbon ($Z = 6$) and oxygen ($Z = 8$), averaged Z is described as

$$Z_{\text{ave}} = 26x + 6(0.8 - x) + 8 \times 0.2 \tag{3}$$

where x is the iron concentration, that is evaluated from the EDS result in Fig. 3, and the oxygen concentration should be constant 20% (actually, this oxygen concentration is not critical because the atomic number of carbon and oxygen is similar). Figure 5a and b show a HAADF-STEM image of the No. 6 nanorod and a line profile of the intensity across the line AA' in Fig. 5a, respectively. From this, it was confirmed that the cross section of the nanorod is approximately elliptic. By comparing the height of the intensity profile of the nanorods, relative thickness of the nanorods can be estimated. Here, by assuming that the thickness of the No. 6 nanorod is 250 nm (e.g., 4450 counts in

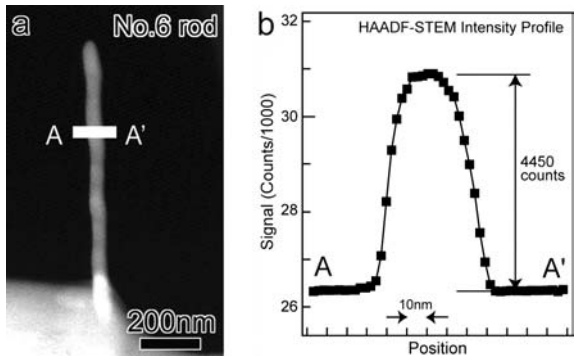

Fig. 5 HAADF-STEM image of the No. 6 nanorod. (**b**) Line profile of the intensity across the line AA' in (**a**)

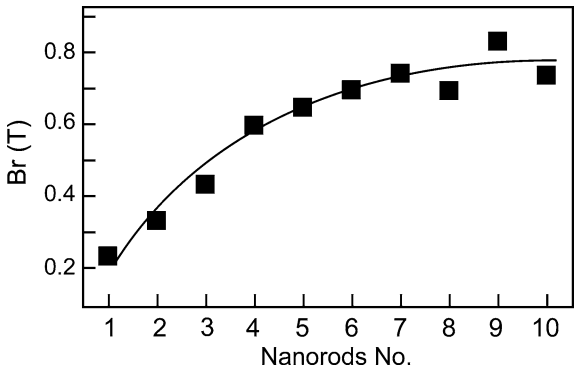

Fig. 6 The remanent magnetic flux density B_r for the No. 1–10 nanorods

Z-contrast intensity corresponds to 250 nm thickness), the thickness for other nanorods can be extracted. Thus, the cross section area S for each nanorod was calculated and consequently the remanent magnetic flux density B_r could be obtained. Figure 6 shows calculated B_r values for the No. 1–10 nanorods, indicating that a fitting curve (solid line) described in the figure is quite similar to a dotted curve (iron concentration) in Fig. 3. It was found that the remanent magnetic flux density B_r of the EBID nanostructures containing iron and carbon is related to the iron concentration.

Conclusions

A FEG-SEM equipped with a dual gas introduction system was developed to fabricate nanostructures with different compositional ratio of iron to carbon by EBID with iron carbonyl and ferrocene gases. It was demonstrated that the compositional ratio of iron to carbon in the nanostructures was controlled by changing the partial pressure of these gases. This technique will be applied to fabricate not only composites of carbon and iron but also nanostructures containing combinations of various elements. Off-axis

electron holography was carried out to evaluate the remanent magnetic flux density B_r for the nanostructures with various compositional ratios of iron to carbon, indicating that the B_r value is related to the iron concentration. Iron distribution and microstructure of iron nanocrystals (or amorphous) also would affect magnetic properties of EBID nanostructures containing magnetic elements. The further detailed studies concerning them are currently in progress.

References

1. Li SP, Natali M, Lebib A, Pepin A, Chen Y, Xu YB (2002) J Magn Magn Mater 241:447
2. Otani Y, Pannetier B, Nozieres JP, Givord D (1993) J Magn Magn Mater 126:622
3. Koops HWP, Kretz J, Rudolph M, Weber M, Dahm G, Lee KL (1994) Jpn J Appl Phys 33:7099
4. Utke I, Luisier A, Hoffmann P, Laub D, Buffar PA (2002) Appl Phys Lett 81:3245
5. Van Dorp WF, Van Someron B, Hagen CW, Kruit P, Crozier PA (2005) Nano Letts 5:1303
6. Mitsuishi K, Shimojo M, Han M, Furuya K (2003) Appl Phys Lett 83:2064
7. Takeguchi M, Shimojo M, Furuya K (2005) Nanotechnology 16:1321
8. Shimojo M, Mitsuishi K, Tameike A, Furuya K (2004) J Vac Sci Technol B 22:742
9. Mitsuishi K, Liu ZQ, Shimojo M, Han M, Furuya K, (2005) Ultramicroscopy 103:17
10. Tanaka M, Shimojo M, Mitsuishi K, Furuya K (2004) Appl Phys A 78:543
11. Kunz RR, Mayer TM (1987) Appl Phys Lett 50:962
12. Utke I, Hoffmann P, Berger R, Scandella L (2002) Appl Phys Lett 80:4792
13. Han M, Mitsuishi K, Shimojo M, Furuya K (2004) Phil Mag 84:1281
14. Shimojo M, Takeguchi M, Tanaka M, Mitsuishi K, Furuya K (2004) Appl Phys A 79:1869
15. Takeguchi M, Shimojo M, Furuya K (2005) Jpn J Appl Phys 44:5631
16. Koops HWP, Kretz J, Rudolphm M, Weber M (1993) J Vac Sci Technol B 11:2386
17. Schossler C, Kaya A, Kretz J, Weber M, Koops HWP (1996) Microel Eng 30:471
18. Rotkina L, Lin J-F, Bird JP (2003) Appl Phys Lett 83:4426
19. Lau YM, Chee PC, Thong JTL, Ng V (2002) J Vac Sci Technol A 20:1295
20. Koops HWP, Kaya A, Weber M (1995) J Vac Sci Technol B 13:2400
21. Liu ZQ, Mitsuishi K, Furuya K (2004) J Appl Phys 96:619
22. Tanaka M, Shimojo M, Takeguchi M, Furuya K (2005) J Crystal Growth 275:2361
23. Ryan MF, Eylen JR, Richardson DE (1992) J Am Chem Soc 114:8611
24. Midgley PA (2001) Micron 32:167
25. Biskupek J, Kaiser U, Lichte H, Lenk A, Gemming T, Pasold G, Witthuhn W (2005) J Magn Magn Mater 293:924
26. Hillyard S, Silcox J (1995) Ultramicroscopy 58:6